THE ASTROPHYSICAL JOURNAL, 567:342–353, 2002 March 1

PULSAR SCINTILLATION IN THE LOCAL INTERSTELLAR MEDIUM: LOOP I AND BEYOND

N. D. RAMESH BHAT
National Astronomy and Ionosphere Center, Arecibo Observatory, HC 3 Box 53995, PR 00612

AND

YASHWANT GUPTA
National Centre for Radio Astrophysics, Tata Institute of Fundamental Research, Pune 411 007, India
Received 2001 July 31; accepted 2001 November 5

ABSTRACT

Recent pulsar scintillation measurements from Ooty, in conjunction with those from Parkes and other large radio telescopes, are used for a systematic investigation of the local interstellar medium (LISM) toward the general direction of the Loop I Bubble. For several pulsars, clear evidence is found for an enhanced level of scattering that is over and above what can be accounted for by the enhanced scattering model for the Local Bubble. These results are interpreted in terms of enhanced scattering due to turbulent plasma associated with the Loop I shell. Useful constraints are obtained for the scattering properties of the shell. The inferred value for the scattering measure for the Loop I shell is found to be ~ 0.3 pc m$^{-20/3}$. Assuming a shell thickness of $\sim$5–10 pc, this implies an average strength of scattering in the shell that is $\sim$100–200 times larger than that in the ambient ISM. An alternative explanation, where the enhanced level of scattering is due to a possible "interaction zone" between the Local Bubble and the Loop I Bubble, is also considered; it is found to be somewhat less satisfactory in explaining the observations. The best-fit value for the scattering measure for such an interaction zone region is estimated to be ~ 1.1 pc m$^{-20/3}$. Furthermore, several pulsars beyond ~ 1 kpc are found to show enhanced levels of scattering over and above that expected from this "two-bubble model." For some of the low-latitude pulsars, this is found to be due to enhanced scattering from plasma inside the intervening Sagittarius spiral arm. We discuss the implications of our results for the interpretation of scintillation data and for the general understanding of the LISM.

Subject headings: ISM: bubbles — ISM: general — ISM: structure — pulsars: general

1. INTRODUCTION

The interstellar medium (ISM) within a few hundred parsecs of the solar system has been a topic of considerable observational and theoretical investigation over recent years (e.g., Breitschwerdt, Freyberg, & Trümper 1998; Frisch 1996; Cox & Reynolds 1987). This region, often referred to as the local interstellar medium (LISM), is known to contain several major features in the form of bubbles, supernova shells, and H I clouds. The solar system itself is thought to reside in a low-density, X-ray–emitting cavity of a mean radius $\sim$100 pc, a region usually referred to as the Local Bubble (e.g., Cox & Reynolds 1987). It is believed to be the remnant of a supernova explosion that occurred $\sim 10^7$ yr ago. Prominent amongst other features in the LISM are the four large-diameter, almost circular rings seen in the all-sky distribution of radio continuum emission. These are appropriately named Radio Loops I to IV (Haslam, Khan, & Meaburn 1971) and are thought to be the projections of quasi-spherical bubbles. Of these, the Loop I Bubble—the largest in angular extent (solid angle $\sim \frac{7}{6}\pi$ steradian) and also the brightest of the four loops—is of special interest (see Salter 1983 for a review). Its close proximity to the Sun allows an in-depth study; see for example, the work of Egger (1993) using data from the *ROSAT* Soft X-Ray Diffuse Background Survey and that of Nishikida (1999), who combined the *ROSAT* Position Sensitive Proportional Counter (PSPC) data with *IRAS* Sky Survey and radio 21 cm data. In terms of origin, Loop I is thought to be an expanding superbubble triggered by an epoch of star formation in the Sco-Cen association some $\sim 10^6$ yr ago. Further, it has been postulated that the properties of the LISM may well be conditioned by the outer shock wave of this supernova remnant (Frisch 1981, 1996; Lallement 1998). Besides these radio loops, the other well-known examples of nearby bubbles that may be important in understanding the LISM are the Eridanus bubble (distance from the Sun $D \sim$ 100–150 pc), the Gum Nebula ($D \sim$ 200–250 pc), the Orion Bubble ($D \sim$ 455 pc), and the Monogem ring ($D \sim$ 100–1300 pc).

Recent X-ray and UV data from *ROSAT* have led to several new insights into the structure of the LISM. A noteworthy result comes from ROSAT PSPC data suggesting an ongoing interaction between the Local Bubble and the Loop I Bubble. By comparing the diffuse X-ray background maps (in the 0.1–2.0 keV band) from the ROSAT All-Sky Survey (Trümper 1983) and H I data over a $160^\circ \times 160^\circ$ region centered at $(l, b) = (329^\circ, +17^\circ.5$; the apparent center of the Radio Loop I), Egger & Aschenbach (1995, hereafter EA95; see also Egger 1993, 1998) recognize a "ringlike" structure between the Local Bubble and Loop I, where the H I column density ($N_{\rm H}$) is even higher than that of the intervening dense H I shell known to exist in the direction of the Sco-Cen OB association (Centurion & Vladilo 1991). From absorption-line studies of nearby stars, the distance to this interaction feature (where $N_{\rm H}$ jumps by nearly an order of magnitude) is estimated to be $\sim$70 pc (see EA95), quite comparable to the distance to the neutral H I wall ($\sim 40 \pm 25$ pc) inferred from *ROSAT* Wide Field Camera star counts (Warwick et al. 1993) and optical and UV spectral line data (Centurion & Vladilo 1991). Interestingly, the formation of such a ring and the inferred density enhancement (by a factor of $\sim$25) are in good agreement with the

numerical simulations of colliding interstellar bubbles (Yoshioka & Ikeuchi 1990). In this picture, Loop I is considered to be an active superbubble, with at least one bubble having already formed a dense cool shell prior to collision. However, alternative interpretations do exist (e.g., Frisch 1996, 1998), wherein the Local Bubble is pictured as an appendix of Loop I. More data and modeling may help to distinguish clearly between the different scenarios.

While much of our understanding of the structure of the LISM comes primarily from X-ray and UV data, nearby pulsars are promising tools for enhancing this understanding. Studies of dispersion and scattering of the radio signals from pulsars are useful means for probing the intervening ISM. Of these two, interstellar scintillation (ISS) effects are more likely to be influenced by the peculiar distribution of the ionized plasma along the line of sight (LOS)—such as clumps of enhanced density superposed on a uniform distribution of ionized material. This is mainly because of (*a*) the nonlinear relation(s) of the scintillation properties to the electron density and (*b*) the fact that scintillation effects depend critically on the relative location of the scatterer (or more generally, the actual distribution of scattering plasma along the sight line). For instance, if the medium is inhomogeneous, in order to produce noticeable effects in the dispersion measure, the density at the clumps has to be considerably larger than to produce similar effects in the scintillation data. However, if the pulsar happens to lie within or near the clumped region, its effect on the scintillation properties could be significantly reduced. Thus, in some sense, dispersion and scintillation data can provide information complementary to each other. Nevertheless, factor *b* would imply that the interpretation of scintillation data is less immune to distance errors and, hence, offers a better handle.

It is quite plausible that the distribution of ionized plasma in and around large local features such as the Local Bubble and Loop I can considerably influence the dispersion and scintillation of nearby pulsars, and in some cases even scintillation of extragalactic radio sources. The large-scale distribution of free electrons and turbulent scattering plasma in the Galaxy has been modeled by Taylor & Cordes (1993, hereafter TC93). While sophisticated compared to its predecessors, the TC93 model takes very little account of the peculiar properties of the LISM due to individual interstellar features. Recent years have seen an accumulation of observational evidence for the effects of such features in the LISM. Early investigations include the work of Phillips & Clegg (1992), who proposed that the scattering of radiation from the nearby pulsar PSR B0950+08 is probably dominated by weakly turbulent plasma present in the interior of the Local Bubble, and that of Hajivassiliou (1992), who invoked an ellipsoidal envelope of highly turbulent plasma to explain the directional anisotropy seen in the turbulent intensity maps derived from interplanetary scintillation studies of radio sources. Even earlier, Rickard & Cronyn (1979) had suggested scattering from the outer shell of Loop I as the plausible cause of a statistically significant lack of interplanetary scintillators seen in a band some 20° outside the brightest section of the Loop I radio emission, the North Polar Spur (NPS).

In a previous paper (Bhat, Gupta, & Rao 1998, hereafter BGR98), we presented a detailed, systematic study of the LISM using pulsar scintillation data from the Ooty Radio Telescope (ORT). Our results and analysis strongly support the view that the scattering in the LISM is probably dominated by turbulent plasma at the boundaries of the Local Bubble. We proposed a simple model, wherein the solar system is surrounded by an ellipsoidal shell-like structure, with a size of ~ 100 pc in the Galactic plane and ~ 500 pc in a plane perpendicular to this (Fig. 4). The scattering structure has its center located at ~ 20–35 pc from the Sun toward $215° < l < 240°$, $-20° < b < +20°$. In this picture, the interior of the bubble is filled with plasma of relatively low turbulence (characterized by a scattering strength $\overline{C_n^2} \sim 10^{-4}$ m$^{-20/3}$), whereas the shell material (thickness ~ 1–10 pc) has a scattering strength ~ 50–800 times larger than that in the ambient ISM (the integrated strength of scattering, scattering measure, is given by $0.11 < \mathrm{SM_{LB}} < 0.28$ pc m$^{-20/3}$). The contribution of the shell thus dominates the total scattering, which would imply that the scattering geometry toward many sight lines can be approximated by a "thin screen" placed at the bubble boundary (location in the range ~ 20–200 pc). This model successfully explained the enhanced level of scattering measured toward a number of nearby pulsars.

The Ooty experiment covered only a few pulsars that would be useful for a study of Loop I. However, the recent results from Parkes observations of a large number of southern pulsars (Johnston, Nicastro, & Koribalski 1998) have significantly improved the ISS data available for probing the ISM in and around Loop I. This motivated us to take a more detailed look at the distribution of scattering material toward Loop I and beyond, a study that forms the main theme of this paper. The paper is organized as follows: § 2 describes observational data and our analysis techniques; § 2.4 and § 2.5 present the modeling of the scattering plasma associated with Loop I. The uncertainties relevant to our analysis are discussed in § 3.1. In § 3.2, we consider some possible alternative models, while later sections of § 3 discuss some general implications of our results for scintillation data and for the LISM. In § 4, we summarize our conclusions.

2. OBSERVATIONAL DATA, ANALYSIS TECHNIQUES, AND MODELING

2.1. *Sample Selection*

For the present analysis, we are interested in pulsars whose scintillation properties are likely to be influenced by the structure of Loop I. In order to preselect pulsars useful for this purpose, we adopt a geometry and size for Loop I from the published literature. Specifically, Berkhuijsen, Haslam, & Salter (1971) derived an angular diameter of $116° \pm 4°$, and a center at $(l, b) = (329.°0 \pm 1.°5, +17.°5 \pm 3.°0$; see also EA95). Furthermore, on the basis of the plausible connection between the origin of Loop I and the Sco-Cen OB association (e.g., Egger & Aschenbach 1995), it is fair to assume the loop center to be near the center of mass of the association (~ 170 pc). Based on the above, we model the Loop I Bubble as a spherical shell of size ~ 290 pc, with the center located at ~ 170 pc toward (329°, 17.°5). This yields 52 pulsars within ~ 2 kpc of the Sun whose sight lines intersect the projected area of Loop I on the sky. On carrying out a literature search, we find scintillation measurements to be available for only 20 of these (see Table 1). The majority of these scintillation measurements are from recent observations with the Parkes and Ooty radio telescopes, while a few are from Arecibo (data from

TABLE 1

PULSAR SAMPLE: THE SCINTILLATION DATA

PSR (1)	l (deg) (2)	b (deg) (3)	D (pc) (4)	$\nu_{d,\mathrm{meas}}$ (MHz) (5)	f_{obs} (MHz) (6)	Reference (7)
J1057−5226.....	286.0	6.6	1530	2.52	660	1
J1430−6623.....	312.7	−5.4	1800	0.28	660	1
J1455−3330.....	330.7	22.6	740	1.37	436	1
J1456−6843[a].....	313.9	−8.5	455	1.4	436	1
J1537+1155.....	19.8	48.3	680	1.53	436	1
J1543−0620.....	0.6	36.6	1160	0.111	327	2
J1544−5308.....	327.3	1.3	1290	6.8	1520	1
J1559−4438.....	334.5	6.4	2000	0.16	660	1
J1603−7202.....	316.6	−14.5	1640	0.36	660	1
J1605−5257.....	329.7	−0.5	1240	20.2	1520	1
J1607−0032.....	10.7	35.5	590	0.379	327	2
J1614+0737.....	20.6	38.2	1500	0.16	436	1
J1709−1640.....	5.8	13.7	1270	0.040	1000	3
J1713+0747.....	28.8	25.2	1100	1.45	436	1
J1730−2304.....	3.1	6.0	510	0.17	327	4
J1744−1134[b].....	14.8	9.2	357	1.34	436	1
J1751−4657.....	345.0	−10.2	1080	0.165	327	2
J1752−2806.....	1.5	−1.0	1530	0.003	1000	3
J1848−1952.....	14.8	−8.3	960	0.23	436	1
J2053−7200.....	321.9	−35.0	1110	0.55	436	1

[a] Interferometric parallax distance from Bailes et al. 1990.

[b] Timing parallax distance from Toscano et al. 1999.

REFERENCES.—(1) Johnston, Nicastro, & Koribalski 1998; (2) Bhat, Rao, & Gupta 1999b; (3) Cordes 1986; (4) Gothoskar & Gupta 2000.

Johnston et al. 1998; Bhat, Rao, & Gupta 1999b; Gothoskar & Gupta 2000; Cordes 1986). The measurements of decorrelation bandwidth ($\nu_{d,\mathrm{meas}}$) and the observing frequencies (f_{obs}) are listed in columns (5) and (6) of Table 1, respectively. The distance estimates in column (4) are derived from dispersion measures (DMs) and the model of Galactic electron density (n_e) by TC93, except for PSRs J1456−6843 and J1744−1134. For these two pulsars, we use independent distance estimates derived from the measurement of annual trigonometric parallax (Bailes et al. 1990; Toscano et al. 1999).

Although the decorrelation bandwidth measurements listed in Table 1 are at different observing frequencies, we have scaled them to a common frequency of 327 MHz, assuming a Kolmogorov scaling law (i.e., a wavenumber spectrum with a slope of 11/3 over the spatial scales of interest: $\nu_d \propto \mathrm{frequency}^{4.4}$). We note that this can potentially produce some errors, as the exact nature of the electron density wavenumber spectrum is still debated. However, there is substantial observational evidence in favor of an $\alpha \approx 11/3$ spectrum toward many sight lines in the LISM (e.g., Bhat, Gupta, & Rao 1999a). Even if this were not strictly correct, most measurements from Parkes will be only marginally affected by an incorrect frequency scaling. This scaling bias may be significant for ν_d values at 1.5 GHz; however, these are for relatively distant objects ($D > 1.2$ kpc) and, hence, less critical for the investigation of scattering in the LISM.

2.2. *Distribution of Scattering: Choice of the Method*

There are three different methods by which pulsar scintillation measurements can be used to investigate the distribution of scattering material in the Galaxy: (1) using the decorrelation bandwidth, ν_d (or its equivalent, the temporal pulse broadening time, τ_p)—this quantifies the scattering measure (SM), which characterizes the total amount of scattering along the LOS. This technique has been used extensively to investigate the large-scale distribution of C_n^2 in the Galaxy (Cordes, Weisberg, & Boriakoff 1985, hereafter CWB85; Cordes et al. 1991; TC93); (2) using measurements of angular broadening (θ_{scatt}) in conjunction with τ_p—wherein the differing weighting functions of the two observables can be used to determine a more exact distribution of C_n^2 along the LOS (e.g., Gwinn, Bartel, & Cordes 1993); (3) using the hybrid method recently proposed by Cordes & Rickett (1998)—wherein the diffractive scintillation measurements (decorrelation bandwidth and scintillation timescale, τ_d), in conjunction with the pulsar proper motion and distance, can be used to obtain the distribution of C_n^2 along the LOS (e.g., Chatterjee et al. 2001).

Of these, method 2 is not relevant in our case, as measurements of θ_{scatt} and τ_p do not exist for bulk of the objects in Table 1. To date, proper motion measurements are known for 9 of the 20 pulsars in Table 1. However, uncertainties are too large for the values to be useful in most cases, and we were unable to derive any meaningful results on the distribution of scattering in and around Loop I. We therefore restricted ourselves to method 1 for the analysis described in this paper (see the Appendix for a detailed description of the method).

2.3. *Comparison with the Local Bubble Model*

We first examine how well the scintillation data in Table 1 agree with the predictions of the Local Bubble model of BGR98, as described in § 1. Figure 1 shows a plot of the ratio of the measured to predicted decorrelation bandwidths ($\nu_{d,\mathrm{meas}}/\nu_{d,\mathrm{pred}}$) against the pulsar distance estimates. We introduce a quantity, ϵ_{all}, that is a measure of the degree

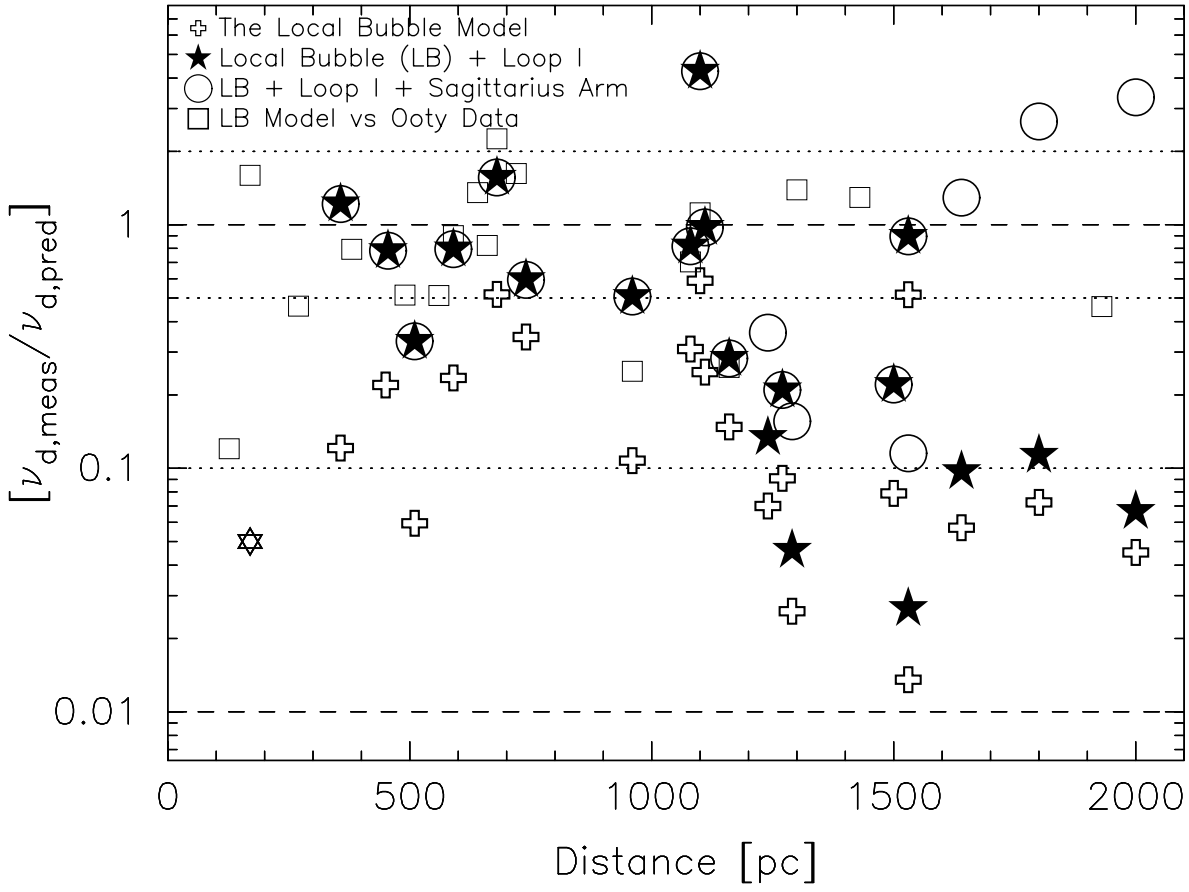

FIG. 1.—Ratios of the measured decorrelation bandwidths ($\nu_{d,\mathrm{meas}}$) to their predictions from the various models for the distribution of scattering in the local ISM ($\nu_{d,\mathrm{pred}}$) are plotted against the distance estimates. The ν_d values are scaled to a common frequency of 327 MHz. The lone unfilled star indicates the measurement of PSR J1744−1134 at its TC93 distance of 166 pc.

of agreement between $\nu_{d,\mathrm{meas}}$ and $\nu_{d,\mathrm{pred}}$. This is expressed as

$$\epsilon_{\mathrm{all}} = \frac{1}{N_p - 1} \sum_{i=1}^{i=N_p} \left[\log \left(\frac{\nu_{d,\mathrm{meas}}}{\nu_{d,\mathrm{pred}}} \right)_i \right]^2 , \qquad (1)$$

where N_p is the total number of pulsars for which the comparison is being made. The logarithm has been taken to give equal weight to discrepancies that are below and above unity when computing ϵ_{all}.[1]

As is obvious from Figure 1, there are large discrepancies (ranging from a factor of 2 to as much as ~ 50) for the case of the Local Bubble model (*shown by crosses*). Considering that most measurements in Table 1 are *not* from observations averaged over many epochs, a potential explanation for part of these discrepancies may be errors due to long-term refractive interstellar scintillation (RISS) effects (e.g., Gupta, Rickett, & Lyne 1994; Bhat et al. 1999a). However, most discrepancies are considerably larger than the worst case factor of 3–5 that can be accounted for by RISS effects. Moreover, it is striking that all the ratios are less than unity, implying that the scattering strengths are systematically larger than that can be accounted for by the Local Bubble model. Furthermore, a systematic trend with distance is also evident in Figure 1, whereby $\nu_{d,\mathrm{meas}}/\nu_{d,\mathrm{pred}}$ (for the Local Bubble model) tends to lie in the range 0.01–0.1 for pulsars beyond 1.2 kpc, but between 0.1 and 1 for those nearer than this. In contrast, for a sample of pulsars within 1 kpc of the Sun in the complementary sky (shown by the open squares in Fig. 1; cf. BGR98), most ratios fall within a factor of 2–3 of unity. The value of ϵ_{all} for this sample (≈ 0.07) is about 16 times lower than that for the Local Bubble model applied to the current data set ($\epsilon_{\mathrm{all}} \approx 1.1$, as shown in Table 3). The simplest interpretation is that there is yet another source of excess scattering (in addition to the Local Bubble shell) in the general direction of Loop I.

2.4. *Enhanced Scattering from the Shell of the Loop I Bubble?*

A number of previous studies have revealed the existence of strong excess scattering toward several sight lines in the Galaxy (e.g., Moran et al. 1990). In the context of modeling the large-scale distribution of C_n^2 in the Galaxy, Cordes et al. (1991) propose a "clump" component, possibly associated with supernova shocks or H II regions, to explain such unusually high scattering. These are regions of intense turbulence, with the strength of scattering many orders of magnitude larger than that in the typical ISM. However, the mean free paths expected for such clumps are rather large (typically $\sim$5–10 kpc). There seems to be no observational evidence for the presence of any such regions in the LISM. Strong excess scattering may also arise if the sight line to a pulsar intercepts an H II region (e.g., Gupta et al. 1994). To the best of our knowledge, none of the pulsars in Table 1 represents such a situation. Even if the LISM contains

[1] We will use the quantities $\epsilon_{<1\ \mathrm{kpc}}$ and $\epsilon_{>1\ \mathrm{kpc}}$ when referring to those parts of the data that correspond to objects with $D \lesssim 1$ kpc and $D \gtrsim 1$ kpc, respectively.

strong scattering regions that are hitherto unknown, these could be relevant only for a few LOSs, whereas the data in Figure 1 suggest a common source of enhanced scattering for many sight lines. Given the current understanding of the LISM, and also on the basis of the results from our earlier work, we postulate that this enhanced scattering is probably caused by the shell of the Loop I Bubble.

2.4.1. *Modeling the Scattering Due to the Loop I Shell*

Here we try to explain the observed discrepancies in decorrelation bandwidths for nearby pulsars in the direction of Loop I in terms of enhanced scattering from a combination of the Local Bubble and the Loop I Bubble. A full modeling of the problem involves the determination of the parameters characterizing their size and location, and the distribution of scattering in and around them. This was done by BGR98 for the case of the Local Bubble alone. However, in the present case, since we already have a model for the scattering from the Local Bubble and there are very good models for the physical dimensions of Loop I, we do not really need to do such full-blown modeling. Instead, we take the following simpler approach.

First, we assume a scattering model for Loop I that is very similar to the multicomponent model for the Local Bubble, i.e., an interior filled with a plasma of relatively low turbulence (the LOS-averaged strength of scattering, $\overline{C_n^2} \sim 10^{-4.2}\ \mathrm{m}^{-20/3}$) and a dense, highly turbulent shell in which the scattering strength is many times larger than in the ambient ISM that lies beyond Loop I. For this ambient medium, we assume $\overline{C_n^2} \sim 10^{-3.5}\ \mathrm{m}^{-20/3}$ (see BGR98).

Second, as described in § 2.1, the size and structure of Loop I are fairly well constrained by previous work (e.g., Berkhuijsen et al. 1971). We simply adopt these values for characterizing the physical dimensions and location of the Loop I shell in our analysis.

Third, we simplify the problem by assuming the thickness of the Loop I shell (d_{LI}) to be small compared with the pulsar distances involved. The problem then essentially reduces to obtaining the best estimate of the scattering measure due to the Loop I shell [$\mathrm{SM}_{\mathrm{LI}} \equiv \int_0^{d_{\mathrm{LI}}} C^2_{n,\mathrm{LIsh}}(l)dl$, where $C^2_{n,\mathrm{LIsh}}$ denotes the scattering strength inside the shell] that will minimize the discrepancies between $v_{d,\mathrm{meas}}$ and $v_{d,\mathrm{pred}}$. Note that the spherical shell geometry of Loop I implies that $\mathrm{SM}_{\mathrm{LI}}$ should be a function of the LOS or, more precisely, of the angular distance of the LOS from the loop center (Θ). This is because the actual path length through the shell intercepted by the LOS varies with Θ. The effect will be more prominent for sight lines that are close to being "tangential." In the analysis that follows, we will constrain SM as defined for a LOS that is normal to the shell (i.e., along $\Theta = 0$).

Fourth, instead of obtaining a solution that will give a best case minimum for all the pulsars in Table 1, we prefer to solve for the SM of the Loop I shell using only two pulsars, PSRs J1744−1134 and J1456−6843. This is justified on the grounds that (*a*) for many pulsars in Table 1, the distance uncertainties and the large errors in the estimates of the decorrelation bandwidth (due to RISS effects), make it less meaningful to do a global fit, and (*b*) for several pulsars at distances $\gtrsim 1$ kpc, Loop I may *not* necessarily be the *only* source of enhanced scattering, and a global fit for $\mathrm{SM}_{\mathrm{LI}}$ could therefore be perturbed by this effect.

The choice of the above two pulsars is dictated by the following arguments. Both pulsars are heavily scattered (Johnston et al. 1998) and have precise, independent distance estimates from parallax measurements—357^{+43}_{-35} pc for PSR J1744−1134 (Toscano et al. 1999) and 455^{+70}_{-56} pc for PSR J1456−6843 (Bailes et al. 1990). Interestingly, the estimate for PSR J1744−1134 is over twice the value of 166 pc derived from the model of TC93. The independent distance estimates allow the scattering geometry along these LOSs to be fairly well constrained. This is illustrated in Figure 2, where the expected locations of the Local Bubble ($D_{b,\mathrm{LB}}$) and Loop I boundaries ($D_{b1,\mathrm{LI}}$ and $D_{b2,\mathrm{LI}}$) in these directions are clearly marked. The farther boundary of the Loop I shell ($D_{b2,\mathrm{LI}}$) lies very close to the midpoint to both objects and is thus optimally placed for maximum contribution to the observed decorrelation bandwidth. Such a geometry will be consistent with the enhanced level of scattering inferred for these two pulsars.

The Appendix describes our method for computing the expected decorrelation bandwidth ($v_{d,\mathrm{pred}}$) for a given distribution of the scattering material along the LOS. We note that if homogeneously distributed scattering material (i.e., eq. [A1], with the integral replaced by $\overline{C_n^2} D$, where $\overline{C_n^2}$ denotes the LOS-averaged strength of scattering) were to explain the observed scattering for the LOSs of these pulsars, the implied level of scattering strength ($\overline{C_n^2} = 10^{-2.8}\ \mathrm{m}^{-20/3}$ toward PSR J1744−1134, obtained from the value reported by Johnston et al. [1998], after scaling for the new distance) would be several times larger than that expected for the typical ambient ISM. This seems quite unlikely. The LISM as relevant to the Local Bubble model of BGR98 can be treated as an inhomogeneous scattering medium, which can be best represented by multiple components of different strengths of scattering (C_n^2) along the LOS (see eq. [A2], for example). This can be represented by a simpler, modified version of equation (A2) (i.e., the right-hand side consisting only the first two integrals and the last integral with the lower limit, $D_{b2,\mathrm{LI}} + d_{\mathrm{LI}}$, replaced with $D_{b,\mathrm{LB}} + d_{\mathrm{LB}}$). If we were to attribute the entire excess scattering to material inside the Local Bubble shell (located at $\sim$30–60 pc in this direction; see Fig. 2), then $C^2_{n,\mathrm{LBsh}}$ would have to be over an order of magnitude larger than that derived by BGR98; alternatively, the shell would have to be much more extended in this direction (say, by an order of magnitude). Again, either of these possibilities is rather unlikely, as it would require a drastic change in the proper-

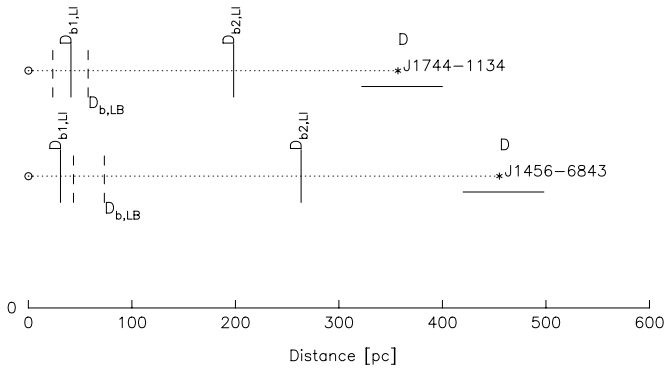

FIG. 2.—Locations of the Local Bubble and Loop I shells along the sight lines toward PSRs J1744−1134 and J1456−6843. The solid lines ($D_{b1,\mathrm{LI}}$ and $D_{b2,\mathrm{LI}}$) indicate the Loop I boundaries, and the dashed lines are the positions of the Local Bubble boundary ($D_{b,\mathrm{LB}}$) that correspond to the two envelopes as shown in Fig. 4. The horizontal bar near the asterisk symbol (*) indicates the uncertainty in the distance estimate of the pulsar.

ties of the Local Bubble in this direction. Hence the possibility that the Loop I shell is the source of the enhanced scattering is most plausible.

We now estimate the optimal value of SM_{LI} by modeling the scattering toward PSRs J1744−1134 and J1456−6843, taking into consideration the scattering due to the Local and Loop I Bubbles, as well as that due to the distributed plasma (i.e., ambient ISM) beyond Loop I. Our model also takes into consideration the characteristic falloff with z-height for the ambient scattering plasma (scale height ~ 500 pc; see TC93), and a Gaussian falloff (scale height ~ 125 pc; see BGR98 for arguments) for the shell material. The interiors of both bubbles are taken to be filled with weakly turbulent plasma ($\overline{C_n^2} \sim 10^{-4.2}$ m$^{-20/3}$). The shell of the Local Bubble is taken to have a scattering measure (SM_{LB}) of 0.2 pc m$^{-20/3}$ (i.e., $\overline{C_n^2} \sim$ a few 100 times larger than that in the ambient medium). The method for computing the expected decorrelation bandwidth ($v_{d,\mathrm{pred}}$) for such a geometry is described by equation (A2) in the Appendix. To determine SM_{LI}, we start with an initial value of 0.2 pc m$^{-20/3}$ and vary this from 0.02 to 2.0 pc m$^{-20/3}$ in steps of 0.01 pc m$^{-20/3}$. Interestingly, the best agreement between the predicted v_d values and those measured is obtained for $SM_{LI} \approx 0.29$ pc m$^{-20/3}$, a value quite comparable to that inferred for the Local Bubble shell.

Using the SM of the Loop I shell, as constrained by the above method, we compute new values for the v_d ratios. These are shown by the filled star symbols in Figure 1. It is quite remarkable that the above modeling successfully removes the discrepancies for pulsars out to a distance of a few 100 pc. The ϵ_{all} value for this model (≈ 0.55) is a significant improvement over that for the earlier model of the Local Bubble alone, as listed in Table 3. Furthermore, as can be seen from this table, there is a dramatic improvement in $\epsilon_{<1\ \mathrm{kpc}}$ (i.e., for pulsars within 1 kpc) and a much smaller one in $\epsilon_{>1\ \mathrm{kpc}}$—exactly as expected for the Local Bubble + Loop I Bubble model.

2.5. *Enhanced Scattering from the Sagittarius Spiral Arm*

Next we address the systematic downward trend for the ratio $v_{d,\mathrm{meas}}/v_{d,\mathrm{pred}}$ in Figure 1 for pulsars beyond ~ 1.2 kpc. A closer examination of these LOSs suggests material within the Sagittarius spiral arm to be the most plausible source of enhanced scattering for several of the pulsars. We show here that these results can be better explained by taking into account the enhanced level of scattering that can be expected due to this spiral arm as per the existing model of TC93. With the arm parameters of the TC93 model and the distance estimates based on this model, the sight lines of six of our pulsars pass through this spiral arm. To model the effect of this, we have simply adopted the arm locations and density parameters of TC93. They consider a squared hyperbolic secant for the z-dependence and a Gaussian falloff for the radial dependence for the arm density, with 300 ± 100 pc for the scale height and 300 pc for the half-width. With an arm density of 0.08 cm^{-3}, i.e., several times larger than the typical $\langle n_e \rangle$ in the LISM, and a fluctuation parameter (F) of 6^{+5}_{-2}, the implied level of scattering is some 2 orders of magnitude larger inside the arm ($C^2_{n,\mathrm{sa}} \sim 0.05$ m$^{-20/3}$) than in the LISM. Hence, substantial amounts of enhanced scattering are expected for these pulsars. On incorporating this, the discrepancies are further reduced (see the open circles in Fig. 1), with a significant improvement in overall agreement ($\epsilon_{\mathrm{all}} \approx 0.22$) as well as for $\epsilon_{>1\ \mathrm{kpc}}$ (see Table 3). The best agreement is seen with the lower and upper limits allowed (by the model of TC93) for the values of the fluctuation parameter and the scale height, respectively.

3. RESULTS AND DISCUSSIONS

We have shown that the combined effect of enhanced scattering from the Local Bubble shell, the Loop I Bubble shell, and the Sagittarius arm goes a long way toward explaining the observed scattering properties of pulsars in the general direction of Loop I. Our new model consists of (*a*) an ellipsoidal shell of SM ~ 0.1–0.3 pc m$^{-20/3}$ to account for scattering due to the Local Bubble, (*b*) a spherical shell of SM ~ 0.3 pc m$^{-20/3}$ to characterize the scattering due to Loop I, (*c*) the ambient ISM ($\overline{C_n^2} \sim 10^{-3.5}$ m$^{-20/3}$) in the interarm region, and (*d*) the Sagittarius spiral arm ($\overline{C_n^2} \sim 0.047$ m$^{-20/3}$). We now discuss some of the implications of these results.

3.1. *Scattering from the Loop I Shell*

The agreement between the measurements and the predictions of our new model is such that the scattering properties of most pulsars out to a distance of 1 kpc are successfully explained ($v_{d,\mathrm{meas}}/v_{d,\mathrm{pred}}$ in the range 0.5–2.0 for 8 out of 10 objects). The major outliers are PSRs J1713+0747 and J1730−2304, with residual discrepancies of ~ 4 and ~ 3 times, respectively, between the predicted and measured values (see Fig. 1) that remain to be explained. These discrepancies are possibly due to RISS, or distance errors, or perhaps as yet unmodeled source(s) of enhanced scattering. For more distant pulsars ($D \gtrsim 1.2$ kpc), although the discrepancies are better accounted for, there still seems to be a systematic downward trend with distance, which is accounted for by extra enhanced scattering due to the Sagittarius arm. The results thus clearly substantiate the role of Loop I as a source of enhanced scattering in the LISM.

We now address the various sources of uncertainties relevant to our analysis. These include (*a*) the uncertainties in size and geometry of (i) the Local Bubble and (ii) Loop I, (*b*) the uncertainty in the (integrated) scattering strength of the Local Bubble (SM_{LB}), (*c*) distance uncertainties, and (*d*) errors on the measurements of v_d. First, we note that the Local Bubble geometry itself is not very well determined (see BGR98), and the expected location of the boundary is in the range ~ 24–58 pc for PSR J1744−1134 and ~ 44–74 pc toward PSR J1456−6843 (see Fig. 4). Taking this into consideration, SM_{LI} could be in the range 0.25–0.3 pc m$^{-20/3}$. However, the uncertainties in the angular size and location of Loop I itself are small (see Berkhuijsen et al. 1971), hence we do not expect them to affect SM_{LI} appreciably. Turning to item *b*, the strength of scattering of the Local Bubble shell (SM_{LB}) itself has a significant uncertainty: $0.11 < SM_{LB} < 0.28$ pc m$^{-20/3}$ (see BGR98). However, this seems to affect SM_{LI} only marginally (0.24–0.32 pc m$^{-20/3}$). The distances to PSRs J1744−1134 and J1456−6843 have $\sim 10\%$ uncertainties, which translate in to a variation of 0.28–0.33 pc m$^{-20/3}$ for SM_{LI}. As for the measurements of v_d, the dominant source of errors are due to their apparent variations caused by RISS effects on timescales from days to weeks. However, these uncertainties are hard to estimate. Nevertheless, if we consider a typical case of a factor of 2 variation in the measured values of v_d, SM_{LI} may lie in the range 0.15–0.57 pc m$^{-20/3}$. Hence, the RISS-induced errors in measured decorrelation bandwidths are

likely to be the dominant source of errors in the final estimate of the strength of scattering of the Loop I shell material.

3.2. *Alternative Scenario: Scattering from an Interaction Zone between the Local Bubble and Loop I?*

In the above analysis, we have attempted to understand the observations in terms of enhanced scattering caused by turbulent plasma within the shells of the two bubbles. Although this two-bubble model seems to successfully explain the scintillation measurements for most nearby pulsars, there is an interesting alternative that deserves consideration. As described in § 1, the work of EA95 and Egger (1998) suggest that the two bubbles are probably undergoing a collision process; the observational evidence for a dense interaction feature at $\sim$70 pc toward Sco-Cen (Fig. 4 of EA95) supports this. Interestingly, the expected location of the closer boundary of Loop I ($D_{b1,\mathrm{LI}}$) is either within the range of or near the Local Bubble boundary ($D_{b,\mathrm{LB}}$) as constrained by BGR98 (see Fig. 4). In particular, for several LOSs, $D_{b1,\mathrm{LI}}$ lies in between the smaller and larger boundaries ($D^a_{b,\mathrm{LB}}$ and $D^b_{b,\mathrm{LB}}$ respectively) of the Local Bubble. The possibility of enhanced scattering from an "interaction zone" between the two bubbles is therefore worthy of consideration.

To examine this possibility, we consider a model where the measured level of enhanced scattering is *entirely* attributable to an "interaction wall" or "zone" whose effective location is at the mean distance of the LB and Loop I boundaries. The two extreme possible geometries for the LB would thus imply two possible locations for the interaction zone (IZ): $D^a_{b,\mathrm{IZ}} = 0.5(D^a_{b,\mathrm{LB}} + D_{b1,\mathrm{LI}})$ and $D^b_{b,\mathrm{IZ}} = 0.5(D^b_{b,\mathrm{LB}} + D_{b1,\mathrm{LI}})$, which correspond to the cases of nearer and farther boundaries of the LB, respectively. These are listed in column (5) of Table 2 ($d_{b,\mathrm{IZ}} = D_{b,\mathrm{IZ}}/D$). In the discussion below, we will refer to these as the IZ-A and IZ-B models, respectively. We also assume that the thickness of this zone (d_{IZ}) is comparable to that of the LB or LI shell, and also that it is much smaller than the pulsar distances. Furthermore, as in the case of the Loop I shell, the path length of the sight line through a possible interaction zone region, and consequently its contribution to the scattering measure, will be a function of the angular distance of the LOS from the loop center. In order to determine the scattering measure of the IZ ($\mathrm{SM_{IZ}}$), we performed a rather similar analysis to that described in § 2.4.1, in which PSRs J1744$-$1134 and J1456$-$6843 are used to estimate the value for $\mathrm{SM_{IZ}}$. For the IZ-A model ($D_{b,\mathrm{IZ}} = D^a_{b,\mathrm{IZ}}$), the best agreement between the measured and predicted values for v_d is obtained for $\mathrm{SM_{IZ}} \approx 1.12$ pc m$^{-20/3}$, which is $\sim$4 times larger than the value of SM for the Loop I shell and $\sim$4–10 times larger than that for the LB. The required SM for the IZ-B case is somewhat smaller: $\sim$3 times the value for $\mathrm{SM_{LI}}$ and $\sim$3–9 times $\mathrm{SM_{LB}}$. This is mainly due to the relatively farther location of the zone in this case. Using these values for $\mathrm{SM_{IZ}}$, we recomputed new values for $v_{d,\mathrm{meas}}/v_{d,\mathrm{pred}}$. The results for the IZ-A model are shown in Figure 3. The agreement is *not* as good as that achieved with the two-bubble model, as indicated by somewhat larger values for the three ϵ parameters that quantify the level of agreement (see Table 3). On a closer comparison of Figures 1 and 3, it is obvious that the agreement is somewhat poorer for several objects at

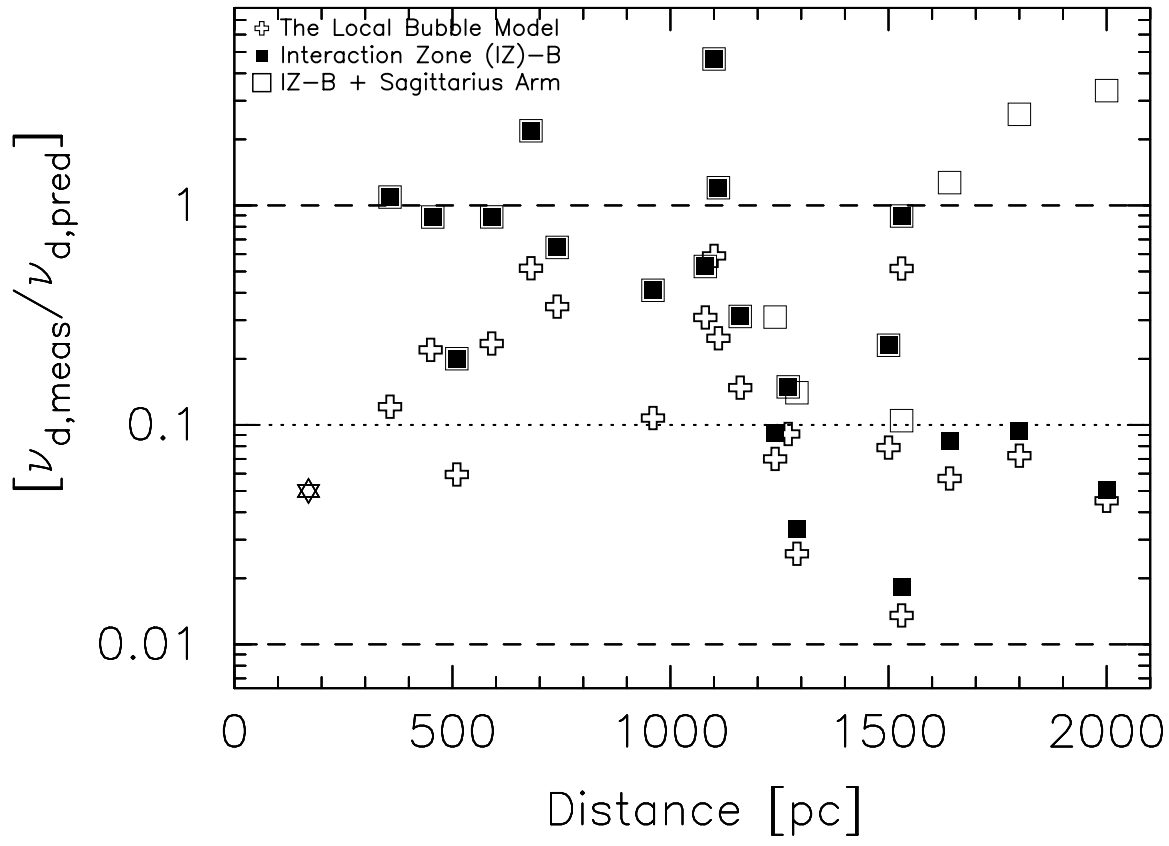

FIG. 3.—Same as in Fig. 1 for the model where the enhanced scattering is due to a possible interaction zone between the Local Bubble and the Loop I Bubble. The results are for $D_{b,\mathrm{IZ}} = 0.5(D^a_{b,\mathrm{LB}} + D_{b1,\mathrm{LI}})$, i.e., for the IZ-A + SA model as described in Table 3 and § 3.2.

TABLE 2

LOCATIONS OF THE LB AND LI BOUNDARIES AND THE IZ

PSR (1)	$d_{b,\mathrm{LB}}$[a] (2)	$d_{b1,\mathrm{LI}}$[b] (3)	$d_{b2,\mathrm{LI}}$[b] (4)	$d_{b,\mathrm{IZ}}$ (5)
J1057−5226.....	0.04–0.05	0.03	0.14	0.03–0.04
J1430−6623.....	0.03–0.04	0.02	0.15	0.02–0.03
J1455−3330.....	0.05–0.10	0.04	0.42	0.04–0.07
J1456−6843.....	0.10–0.16	0.07	0.57	0.08–0.12
J1537+1155.....	0.05–0.12	0.07	0.24	0.06–0.10
J1543−0620.....	0.03–0.06	0.03	0.22	0.03–0.05
J1544−5308.....	0.03–0.05	0.02	0.23	0.02–0.04
J1559−4438.....	0.02–0.03	0.01	0.15	0.01–0.02
J1603−7202.....	0.03–0.05	0.02	0.15	0.02–0.03
J1605−5257.....	0.03–0.05	0.02	0.24	0.03–0.04
J1607−0032.....	0.05–0.12	0.06	0.37	0.06–0.09
J1614+0737.....	0.02–0.05	0.03	0.12	0.03–0.04
J1709−1640.....	0.02–0.05	0.03	0.19	0.02–0.04
J1713+0747.....	0.02–0.06	0.06	0.12	0.04–0.06
J1730−2304.....	0.05–0.12	0.07	0.47	0.06–0.09
J1744−1134.....	0.07–0.16	0.12	0.55	0.09–0.14
J1751−4657.....	0.03–0.06	0.03	0.24	0.03–0.04
J1752−2806.....	0.02–0.04	0.02	0.16	0.02–0.03
J1848−1952.....	0.03–0.06	0.05	0.16	0.04–0.06
J2053−7200.....	0.04–0.08	0.05	0.14	0.05–0.06

NOTE.—Columns (2)–(5) list the fractional distances (e.g., $d_{b,\mathrm{LB}} = D_{b,\mathrm{LB}}/D$).

[a] For the $D_{b,\mathrm{LB}}$ range of the solid and dashed envelopes in Fig. 4.

[b] For the geometry in Fig. 4 [i.e., center located at ∼170 pc from the Sun, toward $(l, b) = (329°, 17.°5)$].

$D \lesssim 1$ kpc. Nevertheless, the IZ model(s) may still be considered as a possible alternative to the two-bubble model. However, unless there are well-studied objects located in the Loop I interior, it is not easy to distinguish conclusively between these two scenarios.

As a natural extension of the IZ model(s), we incorporate scattering due to the Sagittarius spiral arm (as discussed in § 2.5) in order to improve upon the agreement for pulsars beyond 1 kpc with sight lines intercepting that arm. The results for the IZ-A + SA case are shown in Figure 3. The overall agreement, as indicated by $\epsilon_{\mathrm{all}} = 0.27$ and 0.25, respectively, for the IZ-A + SA and IZ-B + SA cases, is somewhat poorer than that achieved with the two-bubble + SA scenario ($\epsilon_{\mathrm{all}} = 0.22$; see Table 3).

3.3. *Discussion*

3.3.1. *Implications of the Results*

Interpretation of the scintillation data.—From the results of this work it is quite evident that the structure of the LISM plays an important role in the interpretation of the scintillation data. The outer shells of the Local Bubble and Loop I may very well be the dominant sources of scattering toward many directions in the LISM, especially at higher Galactic latitudes. Interestingly, independent evidence in favor of similar close-by scattering screens (∼25–250 pc) comes from recent observations of centimeter-wave ISS and intraday variability (IDV) of quasars (e.g., Dennett-Thorpe & de Bruyn 2000; Rickett 2000). In particular, the screen location of ∼25 pc and strength of scattering, $C_n^2 \approx 0.2$ $\mathrm{m}^{-20/3}$, inferred by Dennett-Thorpe & de Bruyn (2000) toward the IDV quasar J1819+3845 is in very good agreement with the location of the Local Bubble boundary (∼25–50 pc) and the scattering strength ($\mathrm{SM}_{\mathrm{LB}}$) expected in this direction. Furthermore, from the work of Hjellming & Narayan (1986), the bulk of the scintillation (RISS) of the radio source PKS 1741−038 at 1.49 GHz is caused by a single screen located at ∼140 pc from the Sun. Interestingly, the LOS to this object ($l = 21.°6$, $b = 13.°1$) lies very close to the "inner ridge feature" of the NPS (beginning at $l \approx 22°$, $b = 14°$). Also, Hjellming & Narayan infer that there is significant excess scattering ($C_n^2 \sim 10^{-1.5}$ $\mathrm{m}^{-20/3}$) along this LOS. Recently, Lazio et al. (2000) report multi-epoch VLBI observations of this object as it underwent an extreme scattering event (ESE); the inferred level of scattering for the ESE lens is orders of magnitude larger than that in the ambient medium. Given the close proximity of the object to Loop I, it is quite probable that the structure(s) that caused the ESE are located at the Loop I shell. Similarly, if an interaction wall between the two bubbles exists, it could potentially act as a thin scattering screen for nearby pulsars with sight lines within $270° < l < 30°$ and $-40° < b < +80°$. Such close-by scattering screens may also explain the shorter than expected timescales seen with the slow intensity variations of pulsars and the low-frequency variables (Gupta, Rickett, & Coles 1993; Spangler et al. 1993). In addition, the enhanced scattering from such bubble shells may be responsible for some of the unusual scattering effects. In this context, it is interesting to note that the location of the scatterer that caused the multiple imaging event of PSR B1133+16 in the Ooty data (Gupta, Bhat, & Rao 1999) was found to match well with the expected location of the Local Bubble shell ($D_{b,\mathrm{LB}} \approx 0.77D$) in this direction. Similarly, it has also been suggested that the structures that cause ESEs in the radio light curves of some quasars are probably associated with the Galactic loops (Fiedler et al. 1994). Recent work by Toscano et al. (1999) and Chatterjee et al. (2001) provides some evidence for enhanced scattering in the third galactic quadrant probably associated with an interface region between the Local Bubble and the GSH 238+00+09 superbubble (Heiles 1998). All of the above arguments clearly support the view that the structure of the LISM needs to be taken into account for a proper interpretation of dispersion and scintillation data.

On the nature of the bubble shells.—In our earlier work (BGR98), we argued that the elongated ellipsoidal shell of

TABLE 3

VARIOUS MODELS CONSIDERED AND THEIR GOODNESS PARAMETERS

Model	Parameters	ϵ_{all}	$\epsilon_{<1\ \mathrm{kpc}}$	$\epsilon_{>1\ \mathrm{kpc}}$
LB	$\mathrm{SM}_{\mathrm{LB}} = 0.2$ + ambient ISM	1.06	0.67	1.41
LB+LI.....	$\mathrm{SM}_{\mathrm{LB}} = 0.2$, $\mathrm{SM}_{\mathrm{LI}} = 0.29$	0.55	0.06	0.90
LB+LI+SA.....	$\mathrm{SM}_{\mathrm{LB}} = 0.2$, $\mathrm{SM}_{\mathrm{LI}} = 0.29$, $C^2_{n,\mathrm{sa}} = 0.047$	0.22	0.06	0.34
LB-LI IZ-A	$\mathrm{SM}_{\mathrm{IZ}} = 1.12$, $D_{b,\mathrm{IZ}} = 0.5(D^a_{b,\mathrm{LB}} + D_{b1,\mathrm{LI}})$	0.68	0.13	1.09
LB-LI IZ-B	$\mathrm{SM}_{\mathrm{IZ}} = 0.83$, $D_{b,\mathrm{IZ}} = 0.5(D^b_{b,\mathrm{LB}} + D_{b1,\mathrm{LI}})$	0.65	0.11	1.06
IZ-A+SA	$\mathrm{SM}_{\mathrm{IZ}} = 1.12$, $C^2_{n,\mathrm{sa}} = 0.047$	0.27	0.13	0.38
IZ-B+SA	$\mathrm{SM}_{\mathrm{IZ}} = 0.83$, $C^2_{n,\mathrm{sa}} = 0.047$	0.25	0.11	0.37

turbulence derived from the Ooty data is possibly associated with the Local Bubble. The analysis described in § 2.4 presents quite convincing evidence for an outer turbulence shell for Loop I also (the existence of a turbulent interaction zone is an alternative possibility, though). Thus, from observational data, it appears that interstellar bubbles in general may have turbulent outer shells.

On the theoretical front, a number of authors have dealt with the evolution of bubbles in the ISM (Ikeuchi 1998 and references therein); in particular, special attention has been paid to the major local features such as the Local and Loop I Bubbles. Interestingly, it turns out that turbulent outer shells can indeed be expected for interstellar bubbles. Specifically, the recent model of Breitschwerdt, Freyberg, & Egger (2000) predicts turbulence to exist at the interface region of the Local and Loop I Bubbles as a natural consequence of the hydromagnetic Rayleigh-Taylor instability caused by the interaction of the two bubbles. A similar mechanism may also apply for the Loop I shell. In an earlier work, Breitschwerdt & Kahn (1988; see also Kahn & Breitschwerdt 1990) showed that turbulent shells could also be expected for stellar-wind–blown bubbles as a consequence of acoustic instability. So, in general, the shells around bubbles may be expected to be turbulent. There are no explicit predictions available for the level of turbulent intensity expected at the shell or in interaction zone regions or for a relation connecting the turbulent intensity to the physical parameters governing the process(es). Nevertheless, the basic results from our investigations using pulsar data appear to be in accordance with some of the theoretical models of bubble evolution.

3.3.2. *Estimation of the Shell Density*

The strength of scattering we derived for the outer shell of Loop I is substantially higher ($\sim$100–500 times depending on the shell thickness) than that measured toward typical LOSs in the LISM. The regions of enhanced electron density (n_e) are also thought to be plausible sites for enhanced scattering (e.g., the Gum Nebula), although the exact relationship between these two is not clearly known. If we consider C_n^2 to be uniform within the shell or the interaction zone regions (i.e., $\mathrm{SM_{LI}} \equiv C^2_{n,\mathrm{LIsh}}\, d_{\mathrm{LI}}$ and $\mathrm{SM_{IZ}} \equiv C^2_{n,iz}\, d_{\mathrm{IZ}}$, where d_{LI} and d_{IZ} represent the path lengths through the shell and interaction zone regions, respectively) and assume a simple relation ($C_n^2 \propto n_e^2$), then an indirect estimate of electron density in the shell ($n_{e,\mathrm{sh}}$) is possible for a given shell thickness. Considering the Loop I shell ($\mathrm{SM} \sim 0.3$ pc $\mathrm{m}^{-20/3}$), for a shell thickness of $\sim$1–10 pc, this yields a density $\sim$10–30 times larger than the ambient ISM value. Somewhat higher values [$\sim(20\text{–}50)\langle n_e\rangle$] result for the interaction zone models described in § 3.2. Interestingly, a similar level of density enhancement is seen for the neutral gas at the annular interface region of the two bubbles (EA95; Egger 1998). For the above densities, the effects on dispersion due to the shell region will be significant only for pulsars within a distance of a few 100 pc. Taking this into consideration would, however, result in a *much lower* ambient density ($\langle n_e\rangle \approx 0.007$ cm^{-3}) toward PSR J1744$-$1134, the disk pulsar with the lowest known n_e. For a similar density enhancement ($\sim$10 times) for the shell region toward PSR J1456$-$6843 (the only pulsar in quadrant 4 with a measured parallax), consideration of shell dispersion would result in an ambient density of $\approx$0.016 cm^{-3} for the two-bubble model and $\approx$0.013 cm^{-3} for the interaction zone model. These values are comparable to $\langle n_e\rangle$ measured toward several objects in quadrant 1 with known parallaxes (see Toscano et al. 1999). Therefore, it is quite plausible that the Loop I shell (or the interaction zone) contributes significantly to the dispersion of nearby pulsars in quadrant 4.

3.3.3. *Electron Densities toward PSRs J1744$-$1134 and J1456$-$6843: Evidence for a Dense Wall?*

It is interesting to note that for the two pulsars—PSRs J1456$-$6843 and J1744$-$1134—with independent distance estimates, the mean electron densities along the sight lines differ significantly: $\langle n_e\rangle$ toward the former is almost twice that for the latter, despite their comparable distances and z-heights (67 and 57 pc, respectively). A closer look at their LOSs vis-à-vis the geometries of the Local and Loop I Bubbles (Figs. 2 and 4) indicates the following: (1) the Local Bubble cavity extends out almost twice as far toward PSR J1456$-$6843 as toward PSR J1744$-$1134 ($\sim$44–74 and $\sim$24–58 pc, respectively, for the geometry in Fig. 4), (2) the interior of Loop I covers a much longer section of the LOS toward PSR J1456$-$6843 ($D_{\mathrm{int}} \equiv D_{b2,\mathrm{LI}} - D_{b1,\mathrm{LI}} \approx 233$ pc for J1456$-$6843, compared to 157 pc for PSR J1744$-$1134; see Fig. 2), and (3) the extent of the ambient medium beyond Loop I is not much larger along the sight line toward PSR J1456–6843 ($\sim$192 pc compared to $\sim$159 pc for PSR J1744$-$1134). All of these make it harder to explain the larger $\langle n_e\rangle$ toward PSR J1456$-$6843.

There appears to be two plausible explanations for the above: (*a*) The ambient ISM in quadrant 4 is simply much denser than that in quadrant 1. However, in the absence of other pulsars in quadrant 4 with measured parallax, there seems to be no independent way to confirm this. (*b*) The existence of a dense interface region between the Local and Loop I Bubbles, as described in § 3.2. On a closer inspection of the sight lines of the two pulsars, case *b* seems the more likely. The LOSs toward PSR J1744$-$1134 intercepts the "annular H I ring," as recognized by EA95 (see also Egger 1998), whereas the LOS toward PSR J1456$-$6843 lies well within the "interaction zone region" confined by this ring-like feature. If the interaction zone region is filled with a denser, highly turbulent plasma, then it could potentially account for much of the dispersion toward PSR J1456$-$6843. If we assume an ambient density of $\approx$0.01 cm^{-3} (i.e., a value comparable to that in quadrant 1), the interaction zone density ($n_{e,\mathrm{IZ}}$) will have to be $\sim$40 times larger in order to account for the excess dispersion. We note that this is quite comparable to the value $\sim(20\text{–}50)\langle n_e\rangle$ derived from the SM estimate as constrained by our modeling. The consistency of the density estimates from the two independent methods can be argued, in some sense, to favor the existence of a dense interaction wall.

Measurements of parallax for other nearby pulsars in quadrant 4 will help to test for the existence of a wall. The most promising candidates for this seem to be low-DM (say, $\lesssim$ 20 pc cm^{-3}) objects with LOSs intercepting the interaction zone region. For instance, PSR J1751$-$4657 would be located much farther ($\sim$1765 pc) than its TC93 distance ($\sim$1080 pc), if the ambient n_e in this quadrant is comparable to that in quadrant 1 ($\sim$0.01 cm^{-3}). PSR J1730$-$2304 (close-by to PSR J1744$-$1134) is another interesting test case, whose distance will only be slightly more ($\approx$555 pc) if a denser zone is present, while it will be located much farther away ($\sim$1 kpc) if the entire sight line was uniformly

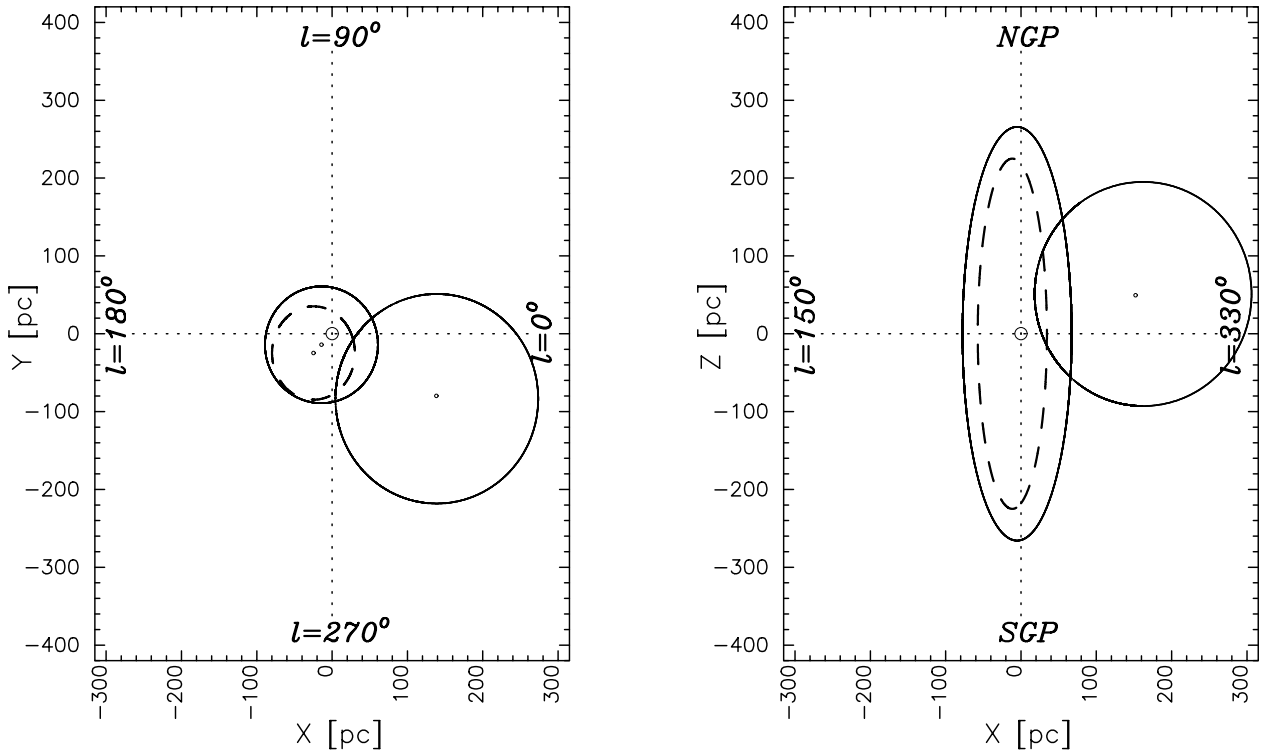

FIG. 4.—Geometry of the Local Bubble and the Loop I Bubble; panel *a* is the section in the Galactic plane, and panel *b* is the section along a plane perpendicular to the Galactic plane and passing through the north and the south Galactic poles, as well as through the center of Loop I. The dashed and solid curves of the elongated cavity correspond to the two different geometries for the local scattering structure as derived from Ooty scintillation data (cf. BGR98).

filled at $n_e \sim 0.01$ cm^{-3}. Similarly, the distance of PSR J1455−3330 will be ∼950 pc (compared to the TC93 value of ∼740 pc) if we consider a dense zone and a low-density (≈0.01 cm^{-3}) ambient medium. While our arguments are based on a fairly simple picture, it is amply clear that measurements of a few interesting test cases will be valuable for understanding the LISM in this quadrant.

3.3.4. *Pulsars and the LISM: Further Prospects*

From the work presented here and related work in the recent past (see § 3.3.1), it is clear that pulsars can be used quite effectively to probe large-scale features in the LISM. Conversely, it is also obvious that detailed interpretation of pulsar dispersion and scintillation data will need to take the structure of the LISM into account. There is growing observational evidence that the Local Bubble is surrounded by numerous bubbles of similar properties, many of which are likely to be filled with hot X-ray–emitting gas. While this work has concentrated on Loop I, our most prominent such neighbor, other nearby examples include the Eridanus bubble, the Gum Nebula, and possibly Radio Loops II and III. Furthermore, there are also observations indicating possible interactions of some of these with the Local Bubble. In this paper, we have considered the possibility of an interaction region between the Local and Loop I Bubbles. Toscano et al. (1999) and Chatterjee et al. (2001) have provided some evidence for interaction of the Local Bubble with the GSH 238+00+09 superbubble in Galactic quadrant 3. The closeness between the location of the near side of the Eridanus Bubble (159 ± 16 pc; Guo et al. 1995) and the expected location of the Local Bubble shell in this direction (≈130 pc) suggests a possible interaction between these two bubbles. The Vela supernova remnant has been shown to be embedded in a hot bubble confined by the shell of the Gum Nebula (Aschenbach, Egger, & Trümper 1995). With the recently revised estimate for its distance (250 ± 30 pc by Cha, Sembach, & Danks 1999), the near side of the "Gum Bubble" is quite close to the Local Bubble boundary (≈100 pc); this is also supported by the observation that the absorbing column density toward the Vela supernova remnant is only about 10^{20} cm^{-2}. An interaction between these two bubbles therefore seems quite likely.

Of the 163 pulsars known within ∼2 kpc of the Sun, scintillation data are presently available for only 73 and independent distance estimates for only 12. Clearly, a lot more needs to be done here. The new generation of large telescopes, such as the Giant Metrewave Radio Telescope and the Green Bank Telescope, could potentially extend the available scintillation data for nearby weak pulsars. For many such cases, measuring pulse-broadening times at low frequencies (≲100 MHz) may prove to be a more viable technique than decorrelation bandwidth measurements. Observations of sources along well-chosen LOSs where the scattering is dominated by the shells of these bubbles may also result in more detections of unusual scattering effects, such as multiple imaging and ESEs. Furthermore, ISS studies of radio sources through centimeter-wave ISS and IDV may also provide useful insights into the nature of the LISM at higher Galactic latitudes. Many such observations hold great promise for extending the rather simplistic models derived from the present investigations into a more realistic picture of the LISM.

4. CONCLUSIONS

We have investigated the distribution of scattering plasma in the LISM in the general direction of the Loop I Bubble by combining recent pulsar scintillation measure-

ments. Many pulsars within ~ 2 kpc, and located toward $270^\circ < l < 30^\circ$ and $-40^\circ < b < +80^\circ$, show enhanced levels of scattering, detected as a significantly reduced value of the ratio of the measured to expected decorrelation bandwidths. The discrepancies cannot be explained by the Local Bubble model (BGR98) alone, and we interpret them as being due to enhanced scattering associated with the shell of the Loop I Bubble and the Sagittarius spiral arm. Using data from two heavily scattered pulsars with precisely known distances, PSRs J1744−1134 and J1456−6843, we have placed useful constraints on the scattering strength associated with the Loop I shell. The scattering measure inferred for the plasma inside this shell is ~ 0.3 pc m$^{-20/3}$, quite similar to that for the Local Bubble shell. Assuming a shell thickness of $\sim$1–10 pc, this implies an average turbulence level $\sim$100–500 times larger than that in the ambient ISM. Adopting this, our earlier model of the LISM is extended by incorporating an explicit scattering component for plasma in and around Loop I, in addition to that due to the Local Bubble. This two-bubble model successfully explains many of the observed decorrelation bandwidth discrepancies for nearby pulsars. The alternative possibility of enhanced scattering from an interaction zone between the Local Bubble and Loop I is also considered. However, the level of turbulence in the interaction zone would have to be several times larger than that for the shells in the two-bubble model in order to explain the observations. Even then, the final agreement with observations for the interaction zone model is not as good as that for the two-bubble model. Assuming a simple relation between the scattering strength and the free electron density ($C_n^2 \propto n_e^2$) yields a shell density that is $\sim$10–30 times larger than the ambient value and a somewhat higher density [$\sim(20$–$50)\langle n_e\rangle$] for the interaction zone model. For several low-latitude pulsars at $D \sim 1$–2 kpc ($|z| \lesssim 300$ pc), we find that the observed scattering discrepancies are consistent with additional enhanced scattering from the Sagittarius spiral arm.

We have discussed implications of our results for the interpretation of scintillation data as well as for the structure of the LISM. In the light of our results and those from several other recent works, we conclude that the structure of the LISM needs to be considered in the interpretation of pulsar dispersion and scintillation data and may also be relevant for observations of centimeter-wave ISS. Furthermore, the general picture that emerges from the investigations in support of turbulent outer shells and/or interface regions of interstellar bubbles appears to be in qualitative agreement with the expectations of the models that describe the evolution of bubbles in the ISM.

We thank C. Salter for several fruitful discussions and valuable comments on the earlier versions of this paper which helped us to improve the content. We also thank P. B. Preethi for help with the analysis software during early stages of this work.

APPENDIX

DECORRELATION BANDWIDTH FOR AN INHOMOGENEOUS, MULTICOMPONENT SCATTERING MEDIUM

Here we describe the method adopted for computing the decorrelation bandwidth ($\nu_{d,\mathrm{pred}}$). Figure 2 depicts typical scattering geometries relevant in our analysis: $D_{b,\mathrm{LB}}$ is the expected location of the Local Bubble boundary, $D_{b1,\mathrm{LI}}$ and $D_{b2,\mathrm{LI}}$ denote the nearer and farther boundaries, respectively, of the Loop I Bubble, and D is the pulsar distance.

For a homogeneous scattering medium, the decorrelation bandwidth (ν_d) is given by (CWB85)

$$\nu_d = \frac{1}{D}\,(A_\alpha\, f_{\mathrm{obs}}^{\alpha})^{2/(\alpha-2)}\left[\int_0^D C_n^2(z)\,dz\right]^{2/(2-\alpha)}, \tag{A1}$$

where A_α is a model-dependent constant, f_{obs} denotes the frequency of observation, and α is the slope of the electron density wavenumber spectrum. In this scheme, the observer is at $z = 0$ and the pulsar at $z = D$. If we adopt the canonical value of 11/3 for α (i.e., a Kolmogorov-like spectrum), $A_\alpha = 2 \times 10^{-6}$.

The LISM model corresponding to Figure 2 can be treated as an inhomogeneous scattering medium, with multiple components of different strengths of scattering (C_n^2, also called turbulent intensity or scattering strength), located at different points along the line of sight. The observable ν_d is determined by the path length differences of scattered rays; therefore, contributions to it from $C_n^2(z)$ need to be appropriately weighted in such a way that scattering regions near the source or the observer produce smaller path-length differences than those that are midway (CWB85). Hence, for the case of our interest, equation (A1) can be rewritten as

$$\begin{aligned}\nu_d = \frac{1}{D}\,(A_\alpha\, f_{\mathrm{obs}}^{\alpha})^{2/(\alpha-2)}\Bigg\{&\int_0^{D_{b,\mathrm{LB}}} w_c(z)C_{n,\mathrm{LBint}}^2(z)\,dz + \int_{D_{b,\mathrm{LB}}}^{D_{b,\mathrm{LB}}+d_{\mathrm{LB}}} w_c(z)C_{n,\mathrm{LBsh}}^2(z)\,dz\Bigg\}\\ &+\int_{D_{b,\mathrm{LB}}+d_{\mathrm{LB}}}^{D_{b1,\mathrm{LI}}} w_c(z)C_{n,\mathrm{ism}}^2(z)\,dz + \int_{D_{b1,\mathrm{LI}}}^{D_{b1,\mathrm{LI}}+d_{\mathrm{LI}}} w_c(z)C_{n,\mathrm{LIsh}}^2(z)\,dz\\ &+\int_{D_{b1,\mathrm{LI}}+d_{\mathrm{LI}}}^{D_{b2,\mathrm{LI}}} w_c(z)C_{n,\mathrm{LIint}}^2(z)\,dz + \int_{D_{b2,\mathrm{LI}}}^{D_{b2,\mathrm{LI}}+d_{\mathrm{LI}}} w_c(z)C_{n,\mathrm{LIsh}}^2(z)\,dz\\ &+\int_{D_{b2,\mathrm{LI}}+d_{\mathrm{LI}}}^{D} w_c(z)C_{n,\mathrm{ism}}^2(z)\,dz\Bigg\}^{2/(2-\alpha)},\end{aligned} \tag{A2}$$

where d_{LB} and d_{LI} are the thickness of Local Bubble and Loop I shells, respectively. The turbulent intensity in the Local Bubble interior and in its shell are represented by $C_{n,\mathrm{LBint}}^2$ and $C_{n,\mathrm{LBsh}}^2$, respectively, and $C_{n,\mathrm{LIint}}^2$ and $C_{n,\mathrm{LIsh}}^2$ are the equivalent

quantities for the Loop I Bubble. The scattering plasma in the ambient ISM is characterized by $C^2_{n,\mathrm{ism}}$. The symbol $w_c(z)$ is the "weighting function" for $C_n^2(z)$ and is given by

$$w_c(z) = \frac{z}{D}\left(1 - \frac{z}{D}\right). \tag{A3}$$

This simple function is symmetric with respect to the midpoint between observer and pulsar, which means an inherent ambiguity is involved in the interpretation of the underlying scattering geometry. For instance, in the simple case of a thin screen placed between us and a pulsar, a screen closer to pulsar (say, at $z = \frac{3}{4}D$) will be equivalent to the one placed at $z = \frac{1}{4}D$ from us. In the case of an extended, inhomogeneous medium (as in Fig. 2), the "inverse geometry" is indistinguishable from the actual geometry.

REFERENCES

Aschenbach, B., Egger, R. J., & Trümper, J. 1995, Nature, 373, 587
Bailes, M., Manchester, R. N., Kesteven, M. J., Norris, R. P., & Reynolds, J. E. 1990, Nature, 343, 240
Berkhuijsen, E., Haslam, C. G. T., & Salter, C. 1971, A&A, 14, 252
Bhat, N. D. R., Gupta, Y., & Rao, A. P. 1998, ApJ, 500, 262 (BGR98)
———. 1999a, ApJ, 514, 249
Bhat, N. D. R., Rao, A. P., & Gupta, Y. 1999b, ApJS, 121, 483
Breitschwerdt, D., Freyberg, M. J., & Egger, R. J. 2000, A&A, 361, 303
Breitschwerdt, D., Freyberg, M. J., & Trümper, J., eds. 1998, IAU Colloq. 166, The Local Bubble and Beyond (Lecture Notes in Physics 506; Berlin: Springer)
Breitschwerdt, D., & Kahn, F. D. 1988, MNRAS, 235, 1011
Centurion, M., & Vladilo, G. 1991, ApJ, 372, 494
Cha, A. N., Sembach, K. R., & Danks, A. C. 1999, ApJ, 515, L25
Chatterjee, S., Cordes, J. M., Lazio, T. J. W., Goss, W. M., Fomalont, E. B., & Benson, J. M. 2001, ApJ, 550, 287
Cordes, J. M. 1986, ApJ, 311, 183
Cordes, J. M., et al. 1991, Nature, 354, 121
Cordes, J. M., & Rickett, B. J. 1998, ApJ, 507, 846
Cordes, J. M., Weisberg, J. M., & Boriakoff, V. 1985, ApJ, 288, 221 (CWB85)
Cox, D. P., & Reynolds, R. J. 1987, ARA&A, 25, 303
Dennett-Thorpe, J., & de Bruyn, A. G. 2000, ApJ, 529, L65
Egger, R. J. 1993, Ph.D. thesis, Tech. Univ. Munchen
———. 1998, in IAU Colloq. 166, The Local Bubble and Beyond, ed. D. Breitschwerdt, M. J Freyberg, & J. Trümper (Lecture Notes in Physics 506; Berlin: Springer), 287
Egger, R. J., & Aschenbach, B. 1995, A&A, 294, L25 (EA95)
Fiedler, R. L., Dennison, B., Johnston, K. J., Waltman, E. B., & Simon, R. S. 1994, ApJ, 430, 581
Frisch, P. C. 1981, Nature, 293, 377
———. 1996, Space Sci. Rev., 78, 213
———. 1998, in IAU Colloq. 166, The Local Bubble and Beyond, ed. D. Breitschwerdt, M. J Freyberg, & J. Trümper (Lecture Notes in Physics 506; Berlin: Springer), 269
Gothoskar, P., & Gupta, Y. 2000, ApJ, 531, 345
Guo, Z., Burrows, D. N., Sanders, W. T., Snowden, S. L., & Penprase, B. E. 1995, ApJ, 453, 256
Gupta, Y., Bhat, N. D. R., & Rao, A. P. 1999, ApJ, 520, 173
Gupta, Y., Rickett, B. J., & Coles, W. A. 1993, ApJ, 403, 183
Gupta, Y., Rickett, B. J., & Lyne, A. G. 1994, MNRAS, 269, 1035
Gwinn, C. R., Bartel, N., & Cordes, J. M. 1993, ApJ, 410, 673
Hajivassiliou, C. A. 1992, Nature, 355, 232
Haslam, C. G. T., Khan, F. D., & Meaburn, J. 1971, A&A, 12, 388
Heiles, C. 1998, ApJ, 498, 689
Hjellming, R. M., & Narayan, R. 1986, ApJ, 310, 768
Ikeuchi, S. 1998, in IAU Colloq. 166, The Local Bubble and Beyond, ed. D. Breitschwerdt, M. J Freyberg, & J. Trümper (Lecture Notes in Physics 506; Berlin: Springer), 399
Johnston, S., Nicastro, L., & Koribalski, B. 1998, MNRAS, 297, 108
Kahn, F. D., & Breitschwerdt, D. 1990, MNRAS, 242, 209
Lallement, R. 1998, in IAU Colloq. 166, The Local Bubble and Beyond, ed. D. Breitschwerdt, M. J Freyberg, & J. Trümper (Lecture Notes in Physics 506; Berlin: Springer), 19
Lazio, T. J. W., et al. 2000, ApJ, 534, 706
Moran, J. M., Greene, B., Rodriguez, L. F., & Backer, D. C. 1990, ApJ, 348, 147
Nishikida, K. 1999, Ph.D. thesis, Pennsylvania State Univ.
Phillips, J. A., & Clegg, A. W. 1992, Nature, 360, 137
Rickard, J. J., & Cronyn, W. M. 1979, ApJ, 228, 755
———. 2000, in IAU Colloq. 182, Sources and Scintillations: Refraction and Scattering in Radio Astronomy, ed. R. Strom & R.-D. Nan (Dordrecht: Kluwer), in press
Salter, C. 1983, Bull. Astron. Soc. India, 11, 1
Spangler, S. R., et al. 1993, A&A, 267, 213
Taylor, J. H., & Cordes, J. M. 1993, ApJ, 411, 674 (TC93)
Toscano, M., et al. 1999, ApJ, 523, L171
Trümper, J. 1983, Adv. Space Res., 4, 241
Warwick, R. S., Barber, C. R., Hodkin, S. T., & Pye, J. P. 1993, MNRAS, 262, 289
Yoshioka, S., & Ikeuchi, S. 1990, ApJ, 360, 352